Fermilab FERMILAB-TM-2124 September 2000

Simulations of the Tevatron Beam Dynamics with Beam-Beam Compensation

D. Shatilov

Budker Institute of Nuclear Physics,

Novosibirsk, Russia, 630090

V. Shiltsev

Fermi National Accelerator Laboratory

P.O.Box 500, Batavia, Illinois 60510

September 1, 2000

Abstract

Compensation of beam-beam effects in the Tevatron proton-antiproton collider by using a counter-traveling electron beam is a subject of on-going experimental project at Fermilab. In this article we present results of numerical tracking of the Tevatron particles in the presence of the beam-beam compensation setup. Our studies cover a wide range of issues relevant to compensation of the bunch-to-bunch tune spread (so called “linear” compensation): electron beam current distribution and size, straightness of the electron beam, misalignment of the electron and antiproton beams, the time to bring the electron and antiproton beams into collision, the effects of noise in the electron beam, and the effect on the proton beam.

1 Introduction

In this article we consider a technique for compensation of the beam-beam effects in the Tevatron with use of high-current, low-energy electron beam [1]. The electron beam setup (TEL = Tevatron Electron Lens) is shown in Fig.1. Currently, the parts of the 1st TEL have been fabricated. Assembly and tests are under way. It is to be installed and used in the Tevatron during Run II (which starts in 2001). The first TEL will be set at F48 (far away from the proton-antiproton interaction points at B0 and D0). It provides a low-energy high-current electron beam which collides with the antiproton beam. The electron beam is created by an electron gun cathode, transported through the region where it interacts with the antiproton bunches while in a strong solenoidal magnetic field. It is then absorbed in the collector. The closed orbit of the proton beam is separated from the electron and antiproton beams in the device.

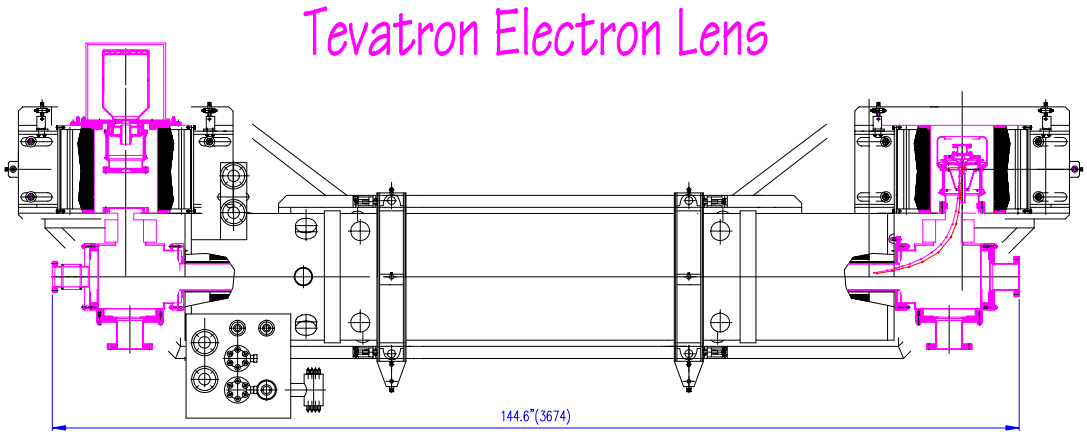

Figure 1: The beam-beam compensation device.

There are two implementations of the beam-beam compensation (BBC) proposal: (i) an "electron lens" with modulated current to provide different linear defocusing forces for different antiproton bunches in order to equalize their betatron frequencies – "linear BBC"; and (ii) an "electron compressor", that is a nonlinear DC electron lens which compensates (on average) the nonlinear focusing of the antiprotons by the proton beam. The numerical studies reported here are mostly focused on "linear BBC".

Due to non-linearity of the primary (proton-antiproton) beam-beam forces and forces between antiproton and electron beams, numerous and potentially dangerous synchrobetatron (SB) resonances can occur at frequencies that in general case satisfy the following relation:

$$n\nu_x + m\nu_y + l\nu_s = \text{integer}. \tag{1}$$

here ν_x, ν_y, ν_s are horizontal, vertical and synchrotron tunes, respectively.

At the moment, nonlinear SB resonances can only be investigated analytically by approximation methods [3] and with use of computer simulations.

We employ developed beam-beam simulation code LIFETRAC for numerical studies effects due to the TEL. Parameters of the collider and a brief description of the code are presented in Section 2. In Section 3 we present results of our studies. Conclusions are summarized in Section 4.

2 BBC Simulations

2.1 Beam-Beam Simulation Code LIFETRAC

The LIFETRAC code was developed for beam-beam simulations in the "weak-strong" model. This model assumes that one beam is much more intensive than the other one. This is consistent with the expected conditions for Run II and TEV33 where the proton bunch intensity is about 4-9 times that of the antiprotons. The "weak" (antiproton) bunch is represented by a number of test particles, while the "strong" (proton) bunch appears as an external force generated by a Gaussian distribution of the charge. Essential features of the code are:

- Arbitrary number of Interaction Points (IP), including Parasitic Crossings (PC), on the ring. Description of each IP (PC) includes: lattice functions (beta, alpha, dispersion), crossing angle, separation (offset) between colliding bunches.
- Fully symplectic 6D synchrobetatron mapping [4], that includes bunch-length effects, slicing of the strong bunch, variation of the beta function β along the bunch during collision, energy change due to longitudinal electric fields.
- Some specific noise sources, which are particularly important for proton colliders: variation of the beams separation at main IPs and fluctuations of the betatron tunes.

The transport transformations between IPs and PCs are assumed to be linear. Focusing lattice nonlinearities, x-y coupling, radiation noise and damping are not taken into account. We exclude these features to simplify analysis of the output, since they are assumed to be less significant for the beam dynamics than beam-beam effects at the IPs and PCs, and the effect of the TELs. In principle, a more realistic lattice can be used in future simulations.

Typically we track 3000 test particles through five slices of strong bunch at the main IPs (at B0 and D0, where β^* is comparable with the bunch length σ_s), and one slice at PCs (where $\beta \gg \sigma_s$). Increasing the number of particles, or the number of slices, gives almost identical results.

The code outputs of the greatest practical utility are luminosity, emittances, and the particle distribution in the space of normalized betatron amplitudes. In general case, the normalized amplitudes are calculated through the normal modes of 6D transport matrix. In the simplified case of 2×2 block-diagonal matrix the normalized betatron amplitude is equal to

$$A_z^2 = \frac{z^2 + (\beta_z z' - \beta'_z z/2)^2}{\sigma_z^2} \tag{2}$$

where z is either x or y and σ_z is the beam size at the observation point. The normal Gaussian distribution, when written for the betatron amplitudes, becomes

$$d\rho(A_x, A_y) = A_x A_y exp(-\frac{A_x^2 + A_y^2}{2}) dA_x dA_y \tag{3}$$

Fig. 2 shows the contour plot for this distribution. The results are generally presented in the same way, a series of contour plots for successive steps, and have to be compared with the baseline results shown in Fig. 2.

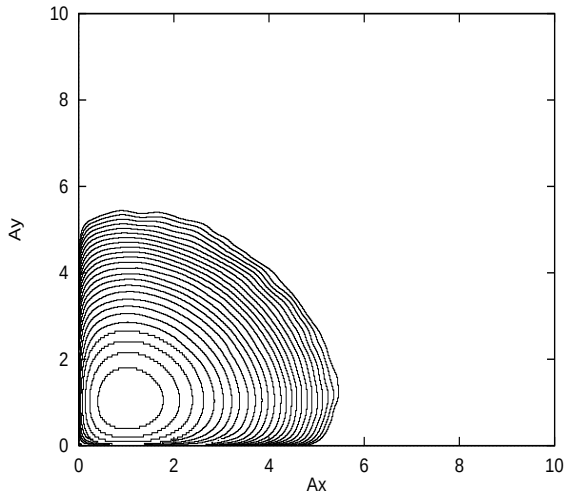

Figure 2: Gaussian distribution in the plane of normalized betatron amplitudes. The distance between successive contour lines is $\sqrt{e}$. Small fluctuations at large amplitudes are due to statistical effects.

The tracking time is divided into a number of steps, usually 10 steps of 300,000 turns. Each step corresponds to about 6 sec of beam time in the Tevatron. The 10 steps corresponds to about 1 min of beam time. It takes about 3 days of CPU time using 20 processors R10000 (SGI) at the Fermilab Farms system. The data gathered during each step are averaged over all the particles and the turns, so we obtain 10 "shots" of $\bar{p}$-beam evolution in time and can observe the growth in both the emittance and the tails.

2.2 Parameters Set

The relevant parameters of the simulations are chosen close to the Run II design ones [5]. The Tevatron focusing lattice variant **v3h15a** has been provided by P. Bagley, its main parameters are presented in the Table 1.

Table 1: Set of beam and accelerator parameters used in simulations.

Energy	E	1000	GeV
$p, \bar{p}$/bunch	$(N_p, N_{\bar{p}})$	(27, 3) $\cdot 10^{10}$	
Number of bunches $(p, \bar{p})$	N_b	36,36	
Number of IPs	N_{IP}	2	
Number of PCs	N_{PC}	70	
Energy spread, rms	$\sigma_{_E}$	$8.7 \cdot 10^{-5}$	
Bunch length, rms	σ_s	37	cm
Synchrotron tune	ν_s	0.001	
Emittance p (normalized)	$\varepsilon_{x,y}$	20	mm·mrad
Emittance $\bar{p}$ (normalized)	$\varepsilon_{x,y}$	15	mm·mrad
Beta-function at IP	$\beta^*_{x,y}$	35	cm
$\bar{p}$ Beam-beam parameter	ξ	0.020	
$\bar{p}$ bunch-to-bunch tune spread	$\delta\nu_{\bar{p}}$	0.007	

The beam-beam parameter for antiprotons is twice (because of two IPs) the zero amplitude head-on beam-beam tune shift: $\xi = 2 \times N_p r_p/(4\pi\gamma\varepsilon_p)$. We should mention that the presented parameters correspond to initial conditions. They are changing in time: e.g., due to noise and intrabeam scattering. Twelve hours after the start of a store the longitudinal and transverse emittances of the proton and antiproton bunches are about 40% larger than their initial values. Due to "burn-up" (loss) of particles because of the collisions and dynamical losses, both beams are about 30% less intense at the end of the store [5, 6].

The beam-beam interaction between protons and antiprotons takes place at the two head-on interaction points located at B0 and D0 sectors, as well as at 70 parasitic crossings where the beam orbits are typically separated by about a dozen of their rms sizes. Since the proton beam intensity is several times the antiproton one, the beam-beam effects are more severe for antiprotons ($\bar{p}$). It is to be noted that the design value of the total tune shift for antiprotons is close to the maximum experimentally achieved value for proton colliders $\Delta\nu \approx 0.025$ [7]. The "footprint area" (spread of betatron frequencies) of the $\bar{p}$-beam with such a tune shift is large enough to also cause an increase of particle losses due to higher order lattice resonances.

Tevatron beam injection requires some gaps in the bunch train that results in the so-called "PACMAN effect" – bunch-to-bunch variation of the betatron tunes due

to long-range beam-beam interactions. The effect depends on the orbit separation around the ring and is most visible for bunches close to the gaps. During Run II with 36 bunches in each beam (3-fold symmetry, 3 trains of 12 bunches), the bunch-to-bunch spread is expected to be about $\delta\nu \approx 0.007$, while the single bunch tune spread due to beam-beam effects at the two main IPs will be about $\Delta\nu \approx 0.018$.

In Ref.[1], it was proposed to use an "electron lens" with modulated current to provide different linear defocusing forces for different antiproton bunches in order to equalize the betatron tunes of the different bunches. Indeed, a round, constant density electron beam with total current J, radius a, and interacting with antiprotons over length L, will produce tune shifts of [1]

$$\xi_z^e = -\frac{\beta_z}{2\pi}\frac{(1+\beta_e)JLr_{\bar{p}}}{e\beta_e c a^2 \gamma_{\bar{p}}}, \tag{4}$$

where $r_{\bar{p}} \approx 1.53 \cdot 10^{-18}$m is the (anti)proton classical radius. For example, one needs an electron beam with $J = 2.35$ A of current along a $L = 2$ m length, with $a = 1$ mm radius, and energy 10 kV ($\beta_e = 0.2$) in order to obtain $\xi^e \approx -0.01$ in the Tevatron collider with parameters $\gamma_p \approx 1066$, β_z=70m. Obviously, two electron lenses – one at a location with the horizontal beta-function larger than vertical $\beta_x \gg \beta_y$, and another one at $\beta_x \ll \beta_y$ can compensate any bunch-to-bunch tune spread. The first one will produce a larger tune shift in the horizontal plane, and the second in the vertical plane. The variable in time electron current can be used for the compensation of the bunch-to-bunch tune spread.

There are two currently designated locations in the Tevatron for two "electron lens" devices – one at the short straight location called F48, and the other at F0. Parameters of these locations are presented in Table 2. Since $\beta_y \leq \beta_x$ at F0, while we want to be $\beta_y \gg \beta_x$, stronger tune shifts (up to 0.021) will be necessary to eliminate bunch-to-bunch tune spread of 0.007.

Table 2: Bunch-to-bunch electron beam lenses

Parameter		F48	F0
Horiz. beta-function,	$\beta^x_{1,2}$, m	101.41	75.76
Vert. beta-function,	$\beta^y_{1,2}$, m	28.46	68.30
Horiz. alpha,	$\alpha^x_{1,2}$	-0.643	-0.554
Vert. alpha,	$\alpha^y_{1,2}$	-0.001	0.393
Horiz. dispersion,	$D_{1,2}$, m	1.748	2.067
Horiz. $\bar{p}$-beam size, rms	$\sigma^x_{1,2}$, mm	0.51	0.46
Vert. $\bar{p}$-beam size, rms	$\sigma^y_{1,2}$, mm	0.26	0.40
Horiz. e- and $\bar{p}$-beams separation,	$S^x_{1,2}$, mm	5.9	2.2
Vert. e- and $\bar{p}$-beams separation,	$S^y_{1,2}$, mm	0.9	1.9
Length of the e-beam,	L, m	2	2

2.3 Simulation goals

The main goal of our simulations is to demonstrate the possibility of using TEL for eliminating the bunch-to-bunch tune spread. Many of physical issues relevant to TEL were studied analytically and reported [1], [3]. Beam-beam simulations allow, in addition, to investigate how TEL affects the nonlinear beam dynamics, and what general conditions (e-beam radius and profile, misalignment, stability, etc.) must be satisfied in order to keep $\bar{p}$-beam stable. We assume here that these conditions should be more or less general, that is do not depend very much on the working point (if it is chosen properly, of course). As an analogy we can mention the well known beam-beam parameter ξ. Many colliders are working with the different tunes and see the different nonlinear resonances limiting their further luminosity increase, but the threshold value of ξ is more or less the same (with the correction on dependence on damping decrements) for all of them.

Although in our simulations we use the lattice close to the real Run II conditions, our goal is neither to find the optimal working point around given area, nor to investigate which resonances are most dangerous and result in growth in the emittance and the tails.

First, we started with simulation of the different bunches in the train to see the bunch-to-bunch tune spread (PACMAN effect) and to test the code. These results are presented in Fig.3. After that, all the simulations were performed for the bunch #6 only. The idea of our study can be expressed as follows:

- Make a small betatron tune scan around the given working point. The tune variations should be about the bunch-to-bunch spread, and the goal was to find some "good" and "bad" working points within this area.
- Apply TEL in the "bad" working point in order to shift it to the "good" one, and see the positive effect.
- Scan some parameters of the TEL and apply some perturbations to see how they affect the resulting $\bar{p}$ distribution.

The most time-consuming part of this work was the last item, where we fixed the working point and the TEL strength (e-beam density), and vary other TEL parameters. Comparison with the natural "good" working point give us important information how the TEL itself introduces perturbations (linear and non-linear) to the $\bar{p}$-beam, and what basic conditions we should satisfy to avoid undesired effects.

Besides, we considered one more question: how the TEL affects the distribution of proton beam (what separation between p-beam and e-beam would be enough to avoid deterioration of the p-beam).

It should be noticed that some parameters, such as amplitudes of the noise, were intentionally chosen large in order to obtain visible effects of $\bar{p}$-bunch degradation

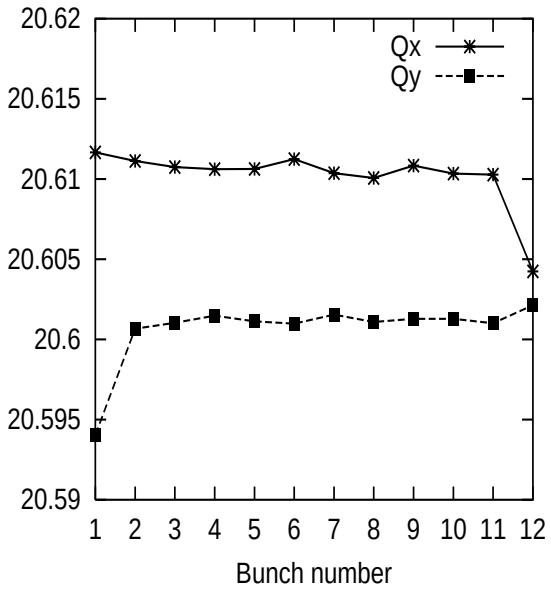

Figure 3: Betatron tunes for the different bunches in the train. The nominal tunes are (ν_x, ν_y)=(20.586, 20.576). The main shifts are due to two IPs with ξ = 0.01, the bunch-to-bunch tune spread is due to PCs.

during limited simulation time (1 minute of the Tevatron real time). A correct approach, with much smaller real noise, would require vast computing resources. However, we believe that proper scaling of the obtained emittance growth rates and particle loss rates can give more or less realistic estimates of the most important effects relevant to the interaction between the TEL and $p, \bar{p}$-beams.

3 Results

3.1 Choice of the working point

We found, after a small tune scan, the working point (20.566, 20.556) to be a good candidate for "bad", and the point (20.556, 20.546) for "good" ones. Here the nominal betatron tunes without beam-beam are presented. To shift from one to another we need only the TEL located at F0, where the beta-functions are approximately equal. The main difference between these two working points is visible on large betatron amplitudes only: there is a "flow" of particles toward large horizontal amplitudes in the "bad" point, that is absent in the "good" one. The distributions in the core region are almost identical, the luminosity decreases by 3-4% in both cases after 10 steps (as a consequence of higher level of noises, see above).

The simulation results are presented in Table 3, where the contour plots are shown. We chose the aperture to be $10\sigma_x$ by $10\sigma_y$, so when a particle achieves the aperture it dies and is not tracked after that. It is important to note that there are big fluctuations at large amplitudes due to statistical errors (small number of particles at these am-

plitudes). The tails decreasing on some steps (for example, 6 to 7 for "bad" point) is a statistical effect from few particles lost at the aperture. Finally, 22 particles from 3000 were lost in the "bad" point and no particle losses were observed in two other cases.

The last column in the Table presents the effect of TEL, which is applied in the "bad" working point and shifts it toward the "good" one. We chose here very big radius of the electron beam (3 mm) just to see the positive effect. The allowable e-beam sizes, as well as other parameters, will be discussed in the next sections.

3.2 Electron beam size and profile

Since the TEL length $L \ll \beta$, transformation through the electron beam can be presented as a single transverse kick depending on the $\bar{p}$-particle coordinates. The kick consists of two parts: electric and magnetic ones. The first one depends on the e-beam distribution density, while the second depends also on the distribution velocity which is not constant due to space charge effects. For tracking purposes, it is convenient to define some function $\rho(r)$ so that the radial kick is equal to:

$$\delta\dot{r} = \frac{\int_0^r \rho(t) \cdot 2\pi t dt}{r} \tag{5}$$

Note that $\rho(r)$ is not a pure distribution density, since it contains also the contribution of the magnetic force.

A *Linear Lens* corresponds to $\rho(r) = const$ for $r \leq R_o$. The e-beam radius R_o must be large enough that all the particles in $\bar{p}$-beam feel the same tune shift, but it is limited by the achievable e-beam current which is proportional to R_o^2. Obviously, the real electron beam has more complicated and "smoothed" profile, which can also be controlled by a special electrode near the cathode [10]. Since e-beam has a low energy ($\beta_e = v_e/c \approx 0.2$), the magnetic contribution to the kick is not significant and can be expressed, in the first order of approximation, by additional small low-order terms in $\rho(r)$. Finally, we decided to use the following formula in our simulations:

$$\rho(r) = \rho_o \frac{1 + a \cdot (r/R_o)^2}{1 + (r/R_o)^8} \tag{6}$$

where a is a "free" parameter modifying the distribution. Functions $\rho(r)$ and $\delta\dot{r}/r$ for R_o = 2 mm and different values of a are shown in Table 4.

In our simulations we first of all scanned R_o with a = 0 to find the minimum acceptable value. In case of R_o = 1 mm (about $2\sigma_{x\bar{p}}$) the $\bar{p}$-beam size grows significantly, so that luminosity decreases by 20% and 28 particles of 3000 were lost. For larger R_o the core region of $\bar{p}$-beam distribution was not disturbed, but the growth of the tails still depends on R_o. The simulation results are presented in Table 5. It is clear that R_o must be at least 1.5 mm (or about 3 times the rms size of $\bar{p}$-beam), otherwise the luminosity lifetime drops dramatically due to both the particle loss and the

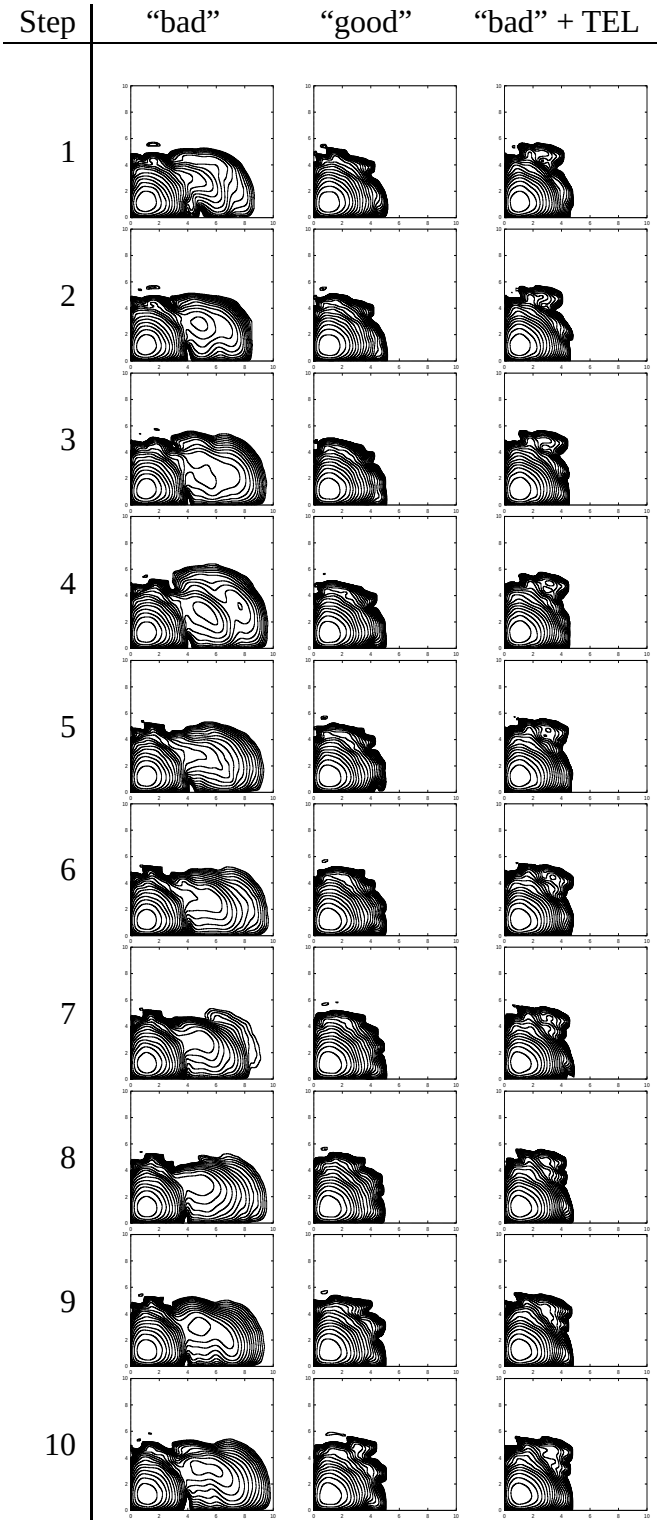

Table 3: Distribution of the $\bar{p}$-beam in the plane of normalized betatron amplitudes. It is clearly seen how the tails grow in the "bad" working point and how TEL shifts it toward the "good" one, improving the situation significantly.

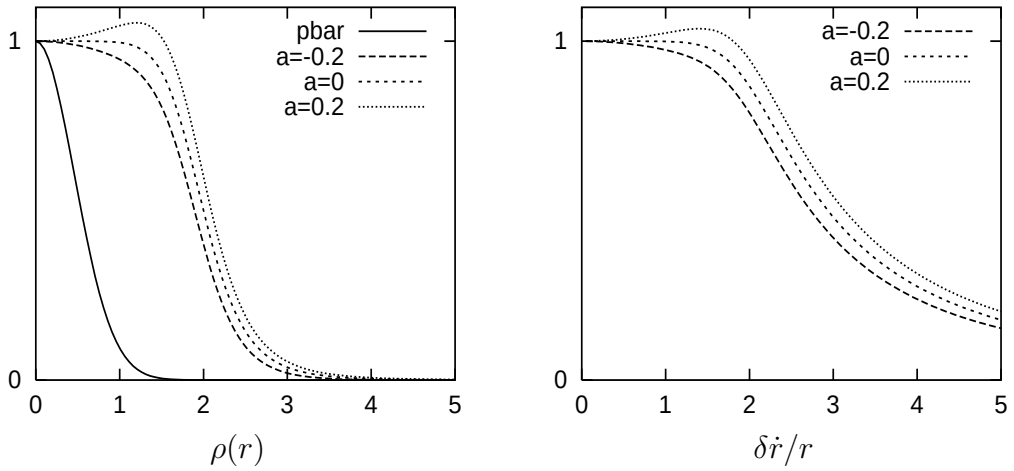

Table 4: Different e-beam profiles and the corresponding radial kicks for R_o = 2 mm and a = [-0.2, 0, 0.2.]. The solid line in left-side figure, marked pbar, shows the profile of $\bar{p}$-beam.

emittance growth. We tried also some other distribution functions, including Gaussian. Fig.4 shows the relative luminosity drop w.r.t. initial luminosity versus total electron current for different distributions. One can see that smoother the distribution, the less luminosity drop we observe (i.e. the Gaussian one is the best of three), but in general the total electron current required to keep the luminosity is approximately the same for all three distribution functions – about 7A to shift the tune by 0.01.

As for $\bar{p}$-beam tails and lifetime, they can be somehow controlled by small modifications of the distribution function $\rho(r)$. In Table 6 we present some selection of the simulation results for different values of a and R_o. As is seen, the case of R_o = 1.5 mm, a = 0.4 is almost equivalent to R_o = 2.0 mm, a = 0. The factor of total e-beam current increase due to a = 0.4 is 1.28, while the same factor for R_o increase from 1.5 to 2.0 mm is 1.78. At the same time, comparing the first two columns (R_o = 2 mm, a = 0, -0.2) we observe the tails shorten together with the electron current decrease (for negative a). Thus we conclude that the effect is very sensitive to the e-beam profile (and, obviously, to the working point) and further optimization can be performed. We have to note, however, that the statistics obtained at large betatron amplitudes were not sufficient. Further studies of the issue with increased number of test particles are necessary.

We have to mention again, that all the parameters correspond to initial conditions, while the antiproton beam size $\sigma_{\bar{p}}$ grows during the many hours of the Tevatron store, and, e.g., the electron beam size should correspondingly grow to match the "$3 \times \sigma_{\bar{p}}$" condition (that can be easily done in the current designs of the TEL magnetic and electron beam systems). Note the p-beam also gets less intense and bigger so that the beam-beam tune shift is also smaller as the store continues.

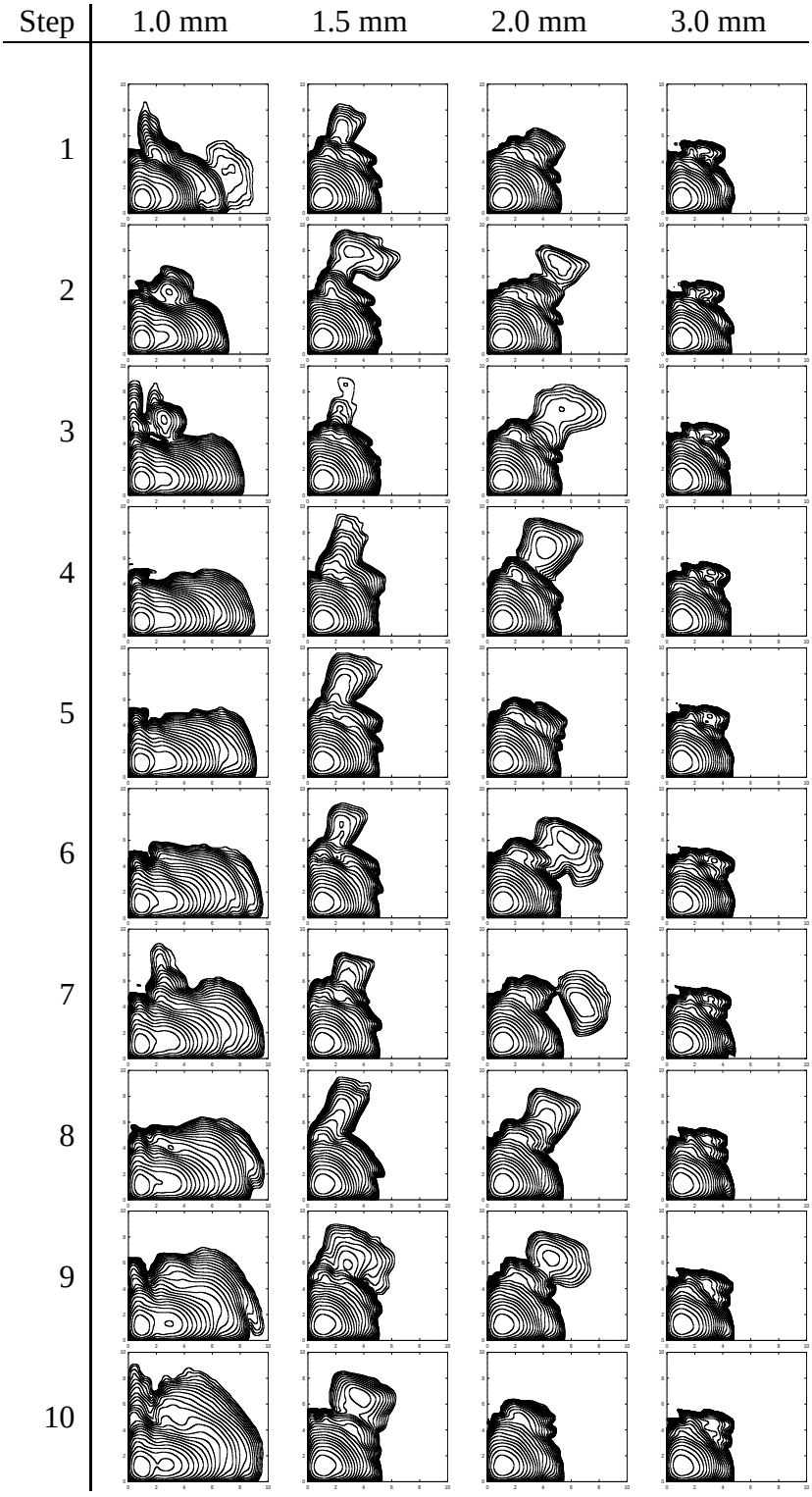

Table 5: Distribution of the $\bar{p}$-beam versus e-beam radius R_o, with a = 0. Luminosity decreases by 20% in the 1st column and about 4% in 2-4 columns. Number of lost particles (from 3000): 28, 15, 4, 0.

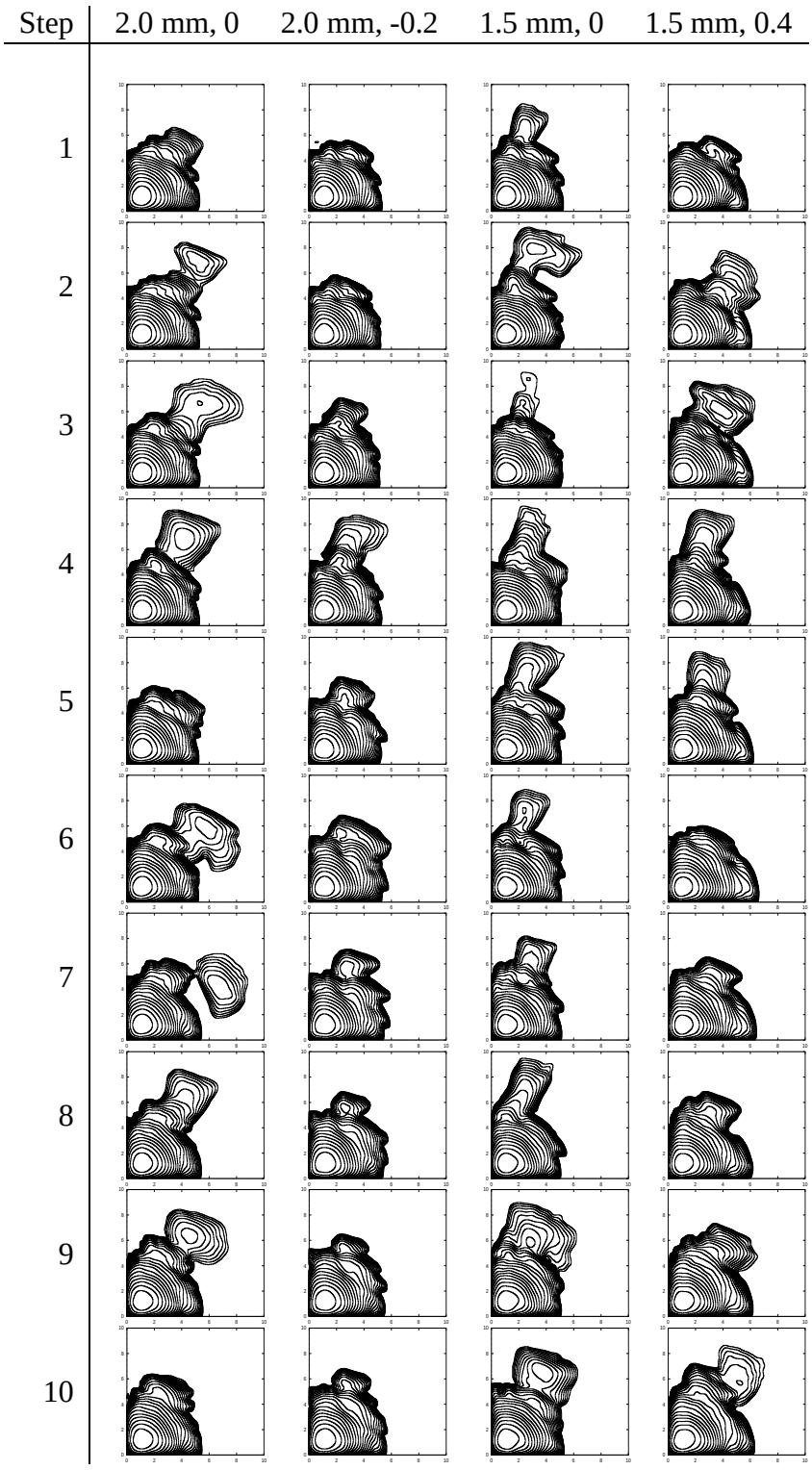

Table 6: Distribution of the $\bar{p}$-beam versus e-beam radius R_o and parameter a. In the 3rd column there is a relatively fast flow of particles to the large vertical amplitudes, that can be recognized by the number of lost particles (from 3000): 4, 1, 15, 4.

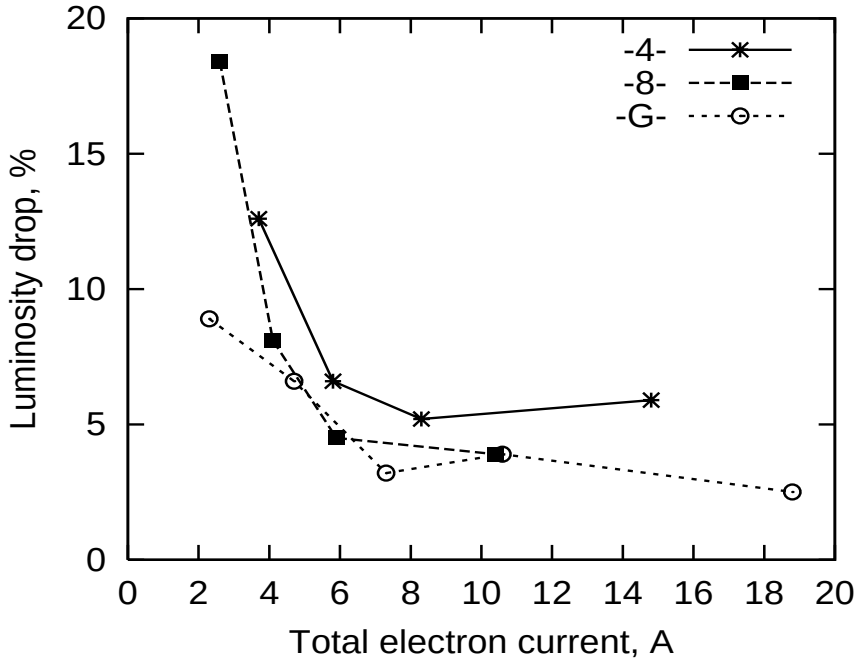

Figure 4: Luminosity drop versus e-beam current for the different profiles. The line marked "4" corresponds to $\rho(r) = \rho_o/(1 + (r/R_o)^4)$, line marked "8" corresponds to $\rho(r) = \rho_o/(1 + (r/R_o)^8)$, line marked "G" corresponds to $\rho(r) = \rho_o \cdot exp(-r^2/2R_o^2)$. These simulations were performed in the very beginning, when we were strongly limited by the computing resources, so we tracked only 300 particles that results in significant statistical errors. However, the need for about 7A of total electron current can be easily recognized.

3.3 Straightness of the electron beam

The electron beam trajectory in the TEL follows strong solenoidal magnetic field lines, and any magnetic error results in e-beam trajectory distortions. Since the effect of the TEL can be reduced to a single transverse kick, any changes in e-beam trajectory are equivalent to some modifications of the distribution function, which becomes now $\rho(x, y)$ (since the x-y symmetry is broken).

In our further simulations we fixed the e-beam distribution parameters to be R_o = 2 mm, a = 0. The intention was do not mix the delicate adjusting of e-beam profile for small (near the threshold) R_o with the other effects under consideration, so we simply increased R_o to get satisfactory conditions. After that we tried a "curved" e-beam with the following horizontal offset between electron and antiproton beams:

$$d_x(z) = d_o \cdot cos(\pi(2z/L - 1)) \tag{7}$$

where z is longitudinal coordinate in the range of 0 to L (solenoid length), d_o = 0.5 mm. Actual magnetic field quality is expected to be within that range or better. Numerical simulations confirmed that it is acceptable and does not worsen $\bar{p}$-beam dy-

namics (losses and emittances).

Moreover, it is worth to mention that variation of the e-beam trajectory by additional orbit correctors (potentially, as many as 20) opens a lot possibilities to control effective integral transverse distribution $\rho(x, y)$. That is especially promising for the future non-linear compensation, but even for linear BBC it can help to adjust e-beam profile in order to shorten the $\bar{p}$-beam tails.

3.4 Misalignment of the electron and antiproton beams

Misalignment of the e- and $\bar{p}$-beams results in a constant orbit shift for antiprotons, and also breaks the symmetry of $\delta\dot{r}$ dependence on the particle coordinates. But the most dangerous effects occur when the edge of electron lens overlaps with the antiproton beam.

Simulations showed that the allowable misalignment can be estimated as a difference between the used value of R_o and its minimum (that is 1.5 mm). So, misalignment of d_x = 0.4 mm was found to be acceptable for R_o = 2 mm: we observed small changes in the tails, but the luminosity, as well as $\bar{p}$-beam lifetime, was not affected. However, for smaller e-beam radius more accurate alignment is required. When we tried R_o = 1.5 mm, a=0.4 (see Table 6, 4th column), we got the luminosity decrease by 4% (that is usual decrease due to noises) for d_x = 0.1 mm and 6% for d_x = 0.2 mm, plus significant tails growth in both cases (10 particles of 3000 were lost). One of the reasons for an increase in the particle loss is that the e-beam profile (a = 0.4) which is optimal for the nominal case may become not so good with misalignments. However, the maximum acceptable value of misalignment can be estimated from the luminosity drop, which is not so sensitive to the profile. Since the vertical $\bar{p}$-beam size $\sigma_{y\bar{p}}$ is smaller at F0 than the horizontal one, greater vertical misalignment is allowed. Judging by our results, the limits for R_o = 1.5 mm are about d_x = 0.1 mm and d_y =0.2 mm, plus additional optimization of the e-beam profile is necessary to reduce the $\bar{p}$-beam distribution tail growth. In any case, the design of the TEL magnetic system includes a number of dipole correctors, so that the electron trajectory can be corrected to coincide with the antiproton orbit in the device.

Nevertheless, the process of bringing two beams into collision can produce damage to the $\bar{p}$-beam. We studied how the resulting distribution depends on the speed of this process. An initial misalignment was chosen to be d_x = 5 mm and decreased exponentially with the time constants τ = 30 and 6 sec, the e-beam radius was R_o = 2 mm, a = 0. The simulation results are presented in Table 7.

The main perturbations $\bar{p}$-beam experiences when overlapping with the edge of electron beam, that corresponds to the shift between beams' centers d_x = 1.5 – 2.5 mm. This occurs on 4 – 6 steps for τ = 30 sec and 1 – 2 steps for τ = 6 sec. Just at these steps we observed the emittance growth and luminosity decrease, after that the beam core remains more or less stable. But the tails continue to grow. It seems, the reason is that many particles already are at some "good" positions for the further

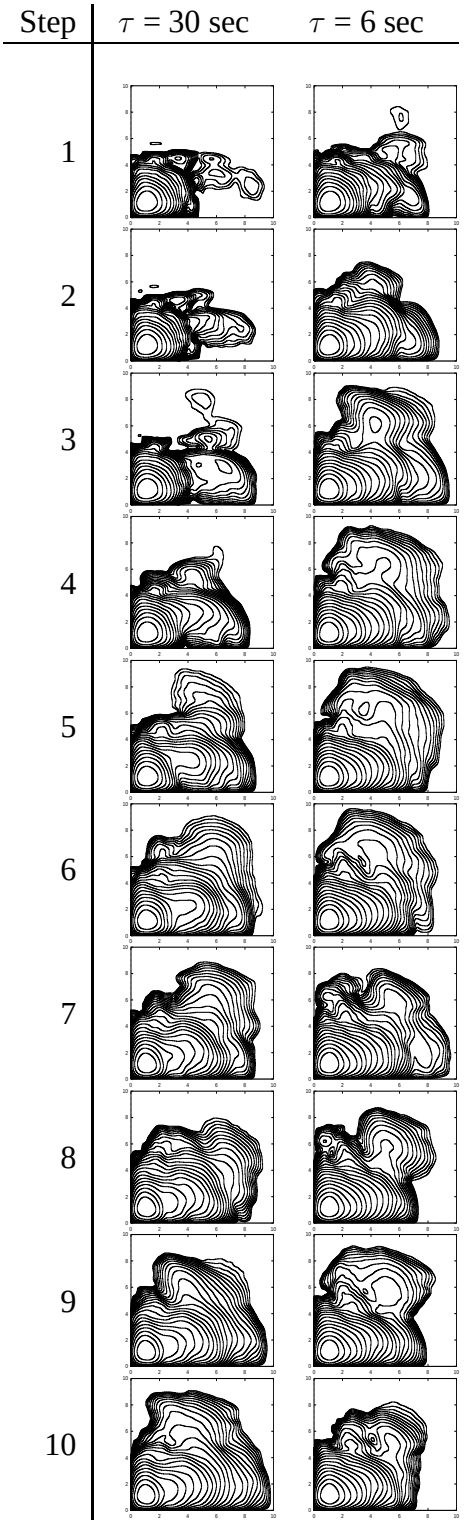

Table 7: Distribution of the $\bar{p}$-beam. The horizontal shift between electron and antiproton beams $d_x(t) = d_o \cdot exp(-t/\tau)$, where d_o = 5 mm, τ = 30, 6 sec for the 1st and 2nd columns, respectively. The luminosity decreases by 10% and 6%, number of lost particles was 36 and 28.

drift, since their amplitudes became large enough to feel the non-linearity of e-beam edges even without any misalignment. However, the process of particle losses is slightly delayed since it takes some time to reach the aperture.

Obviously, the perturbations of antiprotons are unacceptable in both cases. Since the further reduction of τ seems to be impossible, we conclude that alignment of the electron beam, if started with large initial shifts (1-2 mm or more), destroys the antiproton beam. The solution is to perform this operation in few steps, each time injecting new $\bar{p}$-beam, or use smaller electron beam current for initial alignment.

3.5 Effects of the electron beam noises

Random fluctuations of the electron current from turn to turn, as well as transverse motion of the electron beam, cause antiproton emittance growth. Analytical studies of the issue [8], [9] give the emittance evolution equations. The emittance grows exponentially due to electron current fluctuations:

$$\varepsilon_z(t) \approx \varepsilon_{zo} \cdot exp(8\pi^2 t f_o(\xi_{z1}^2 + \xi_{z2}^2)(\frac{\delta J}{J})^2) \tag{8}$$

where z stands for x or y, $\xi_{z1,2}$ are the values of tune shifts produced by two electron lenses, $\delta J/J$ is the rms value of relative current fluctuations. Transverse motion of the e-beam results in linear emittance growth:

$$\frac{d\varepsilon_z}{dt} = 8\pi^2 f_o(\frac{\xi_{z1}^2}{\beta_{z1}} + \frac{\xi_{z2}^2}{\beta_{z2}}) \cdot (\delta Z)^2 \tag{9}$$

where δZ is the rms electron beam vibration amplitude.

Our numerical simulations are in good agreement with these equations, which set strong requirements on the electron beam stability (see, estimates in [1]). So, we got an emittance growth by a factor of 2.2 during 1 min of the beam time with $\delta J/J = 5 \cdot 10^{-3}$, while (8) gives the factor of 1.8. Note that there are also another sources of emittance growth (variation of the beams separation at main IPs, nonlinear effects) resulting in the factor of about 1.2, which is not included in (8).

In future we also plan to improve reliability of these simulations by using more realistic noise spectrum (some specific harmonics emphasized).

3.6 Effects on the proton beam

The proton beam, although separated from the antiproton and electron beams in the TEL, also feels small nonlinear kick due to the electron space charge. Studying the effects on the proton beam we simplified the model by excluding the Parasitic Crossings, on the basis that the antiproton current is several times less than the proton one and the effects due to PCs are negligible for p-beam. So, the one-turn map consists of two IPs at B0 and D0, electron lens at F0 and linear transformations between these

three non-linear elements. The TEL at F0 was chosen by the reason that the separation between e- and p-beams $S_{x,y}$ is smaller at F0 (see Table 2), and therefore the effect is stronger. The radius of e-beam was set to R_o = 1.5 mm, a = 0.

We started with the same "nominal" working point (20.566, 20.556) and the beam-beam parameter ξ_p = 0.002 (which is some 5 times smaller than for antiprotons due to smaller antiproton current), and have not found any problems with p-beam. After that we tried to change some parameters (separation, ξ_p, noises) in order to see their effect. Some selection from these results is presented in Table 8. Columns 3 to 5 correspond to ξ_p = 0.01, that is much greater than in the real conditions, but is useful to improve our understanding. As one can see, the strongest perturbations occur due to "interference" between small separation and big ξ_p. The noises also play a significant role (compare columns 1–2 and 3–4), but only in the presence of the two above factors. Fortunately, the actual value of ξ_p is rather small.

However, even with ξ_p = 0.002 and total separation of 3 mm the situation is not so good as it seems to be, since the effect due to the TEL strongly depends on the working point. It has to be emphasized that the betatron tunes for protons and antiprotons are different, since they feel the different tune shifts from each other and have the different orbits. Obviously, the working point has to be optimized first of all for the $\bar{p}$-beam. Although the betatron tunes for protons and antiprotons can be varied independently using the feed down sextupoles, in our opinion, the "good" result for protons means that p-beam is stable within more or less wide area of betatron tunes. To ensure this, we performed a small tune scan with the nominal parameters: ξ_p = 0.002, total separation of 3 mm (horizontal and vertical, both about 2 mm). In Table 9 we present the simulation results for some "bad" working points found near the nominal one. It is clearly seen that the effect is due to the TEL: the growth of tails starts just at the amplitudes where the two beams overlap. We also tried these working points without TEL and did not find any perturbations.

Finally, we concluded that the separation between e- and p-beams at F0 cannot be considered as sufficient. However, appropriate choice of the working point can solve the problem. As for the TEL located at F48, the separation there is quite acceptable and should not cause any problems.

4 Conclusions

The model of the Tevatron used in our simulations is not quite adequate to the Run II design: the actual variant of the lattice to be used in Run II is subject of continuous changes and most probably the lattice we used is not the final one, no $x-y$ coupling has been taken into account, the "dirt" effects were simplified and chosen intentionally at higher level. However, the main factors affecting non-linear beam dynamics (two interaction points, 70 parasitic crossings, space charge of the electron lens) are considered. Finally, we conclude that our model cannot be rejected as unrealistic, although further studies of the issue are necessary.

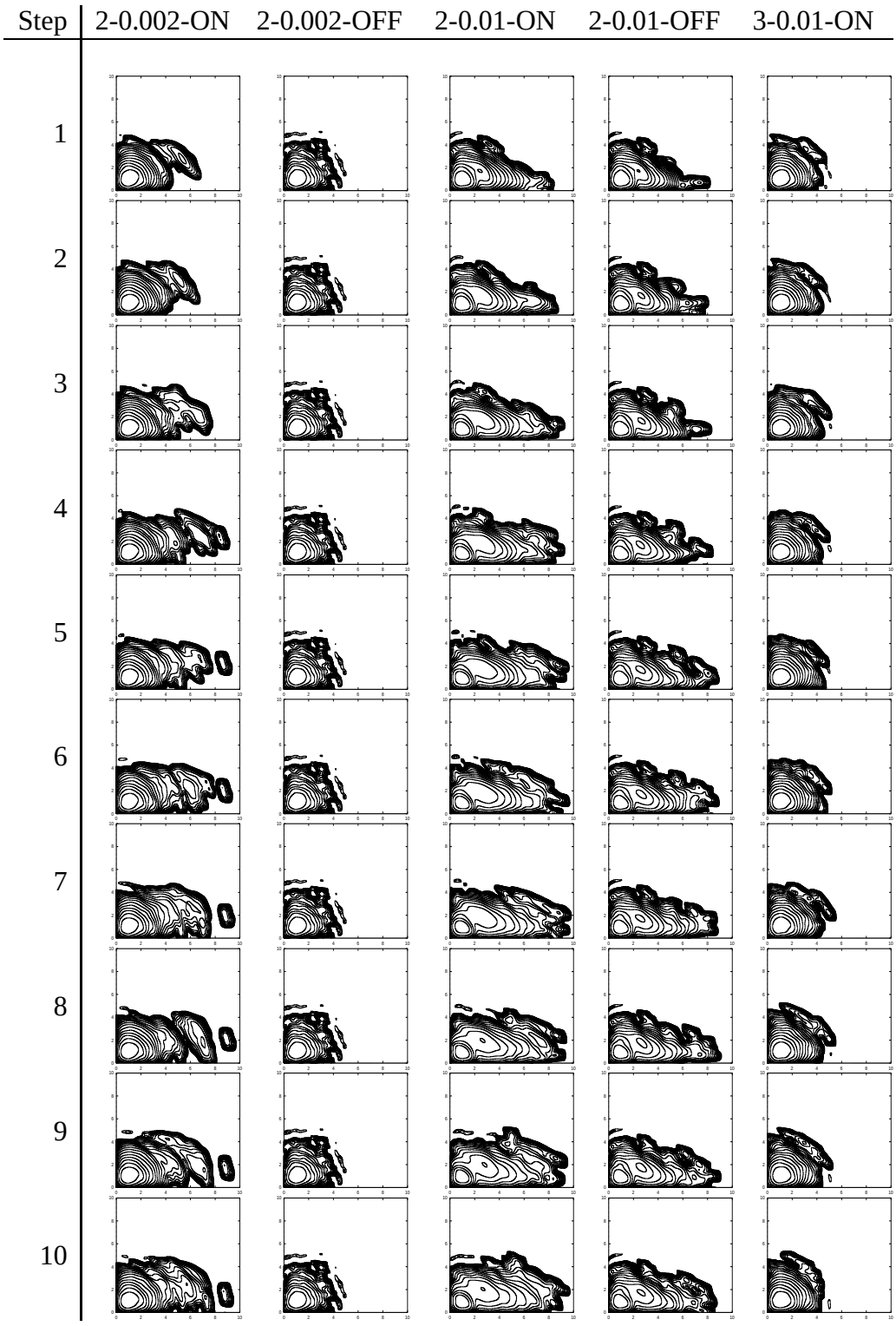

Table 8: Distribution of the p-beam versus separation with the e-beam (mm), beam-beam parameter ξ_p and noises (see legend at the top line). No particle losses were observed in any case.

Step	(.576, .551)	(.571, .561)	(.576, .556)
1	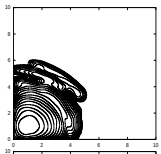	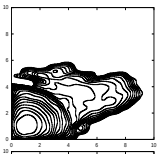	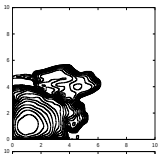
2	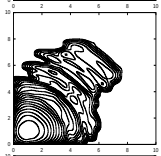	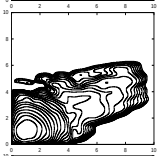	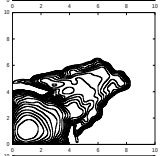
3	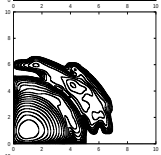	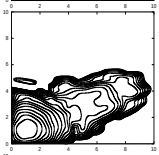	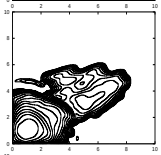
4	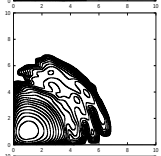	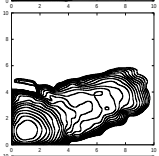	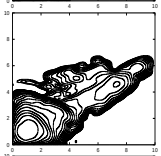
5	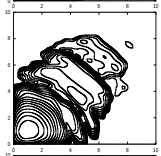	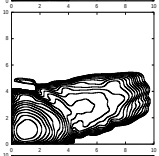	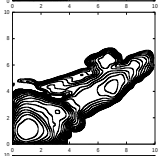
6	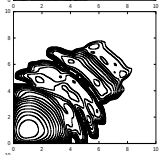	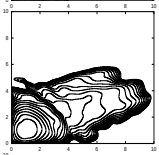	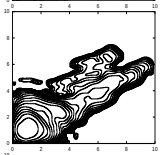
7	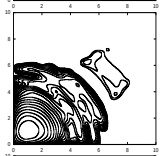	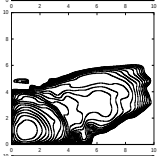	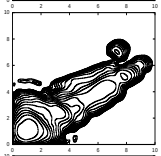
8	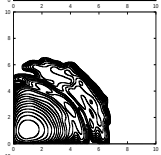	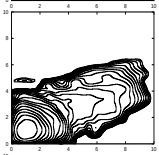	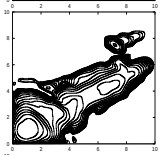
9	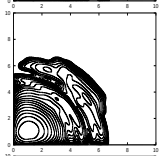	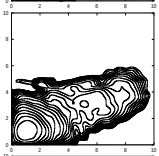	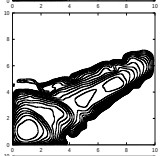
10	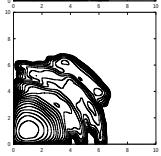	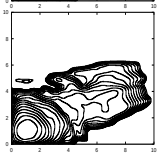	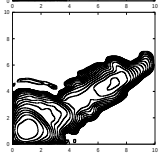

Table 9: Distribution of the p-beam versus the working point. Separation between e- and p-beams is 3 mm, ξ_p = 0.002. Number of lost particles (from 3000): 5, 43, 32.

The major results of this work are:

1. The minimum acceptable value of the electron beam radius R_o is limited by the luminosity degradation (distribution in the $\bar{p}$-beam core) at about 1.5 mm ($3\sigma_{x\bar{p}}$). The tails growth is a separate problem and, if it cannot be solved by an additional R_o increase, can be reduced by modifications of the e-beam profile.

2. The acceptable misalignment of the electron and antiproton beams depends on the e-beam radius and was found to be about 0.5 mm for R_o = 2.0 mm and about 0.1 mm for R_o = 1.5 mm. The process of alignment should be performed with small electron current, otherwise it destroys the $\bar{p}$-beam.

3. The antiproton emittance growth due to electron beam noises was found to be in good agreement with the theoretical predictions.

4. The separation between e- and p-beams at F48 is quite acceptable, while it seems to be insufficient at F0. Appropriate choice of the working point is necessary to solve the problem.

Our further studies will include consideration of the location for the second electron lens for linear beam-beam compensation, studies of the non-linear beam-beam compensation and number of "weak" effects which we omitted in the present studies (dispersion in the TEL, coupling due to lattice and due to electron beam, etc.).

Acknowledgments

We acknowledge valuable comments and fruitful discussions with P. Bagley, N. Gelfand, T. Sen (FNAL) and Yu. Alexahin (JINR, Dubna). We would like to thank the Farms Group in Computer Division at FNAL for the opportunity of using farms for our simulations.

References

[1] V. Shiltsev, V. Danilov, D. Finley, A. Sery, "Compensation of Beam-Beam Effects in the Tevatron with Electron Beams", Phys. Rev. ST Accel. Beams, **2**, 071001 (1999).

[2] P. Bagley, *et.al*,, "Summary of the TeV33 Working Group", FERMILAB-Conf-96/392 (1996).

[3] Yu. Alexahin, "Analytical Study of the Incoherent Beam-Beam Resonances in the Tevatron Run II Lattice with the Beam-Beam Compensation", FERMILAB Pub-00/120-T (2000).

[4] K. Hirata, H. Moshammer and F. Ruggiero, Part. Acc. **40** (1993) 205.

[5] “Run II Parameters, Handbook and Operations”, *http://www-bd.fnal.gov/runII/*.

[6] R. Bharadwaj, *et. al*, “Fermilab Collider Run Ib Accelerator Performance”, FNAL TM-1970 (1996).

[7] G. Dugan, Proc. 1989 IEEE PAC, Chicago (1989), p.426.

[8] G. Stupakov, Report No. SSSL-575 (1992).

[9] V. Lebedev, V. Parkhomchuk, V. Shiltsev and G. Stupakov, Part. Acc. **44** (1994) 147.

[10] A. Shemyakin, et.al, “Performance of a High-Perveance Electron Gun with a Convex Cathode”, Proc. EPAC’00, Vienna (2000).